Plasma Study of a Moly–Oxide–Argon Discharge Bulb

John L. Giuliani, *Member, IEEE*, George M. Petrov, Robert E. Pechacek, and
Robert A. Meger, *Associate Member, IEEE*

Abstract—A mercury-free molybdenum–oxide–argon (Mo–O–Ar) electrodeless discharge is described with potential application to plasma lighting. The low-pressure metallic plasma is a nonequilibrium discharge capable of producing visible light directly with an efficacy of ∼40 lm/W. The Boltzmann equation is solved with a limited set of chemical kinetics to provide a zero-dimensional model of the discharge. Model results indicate a transition in the power transfer from Ar to Mo as the partial pressure of Mo is increased. This feature is qualitatively similar to an intense transition from weak to strong visible emission observed in the Mo–O–Ar discharge with increasing power. The Mo partial pressure at the transition is estimated from an actinometry approach including a collisional radiative model of the plasma. The calculated electron density is also compared with interferometric data.

Index Terms—Excitation dynamics, kinetic models, low pressure discharge, metal–oxide plasmas, plasma lighting.

I. INTRODUCTION

DUE to the potential for environmental regulations, there has recently been substantial interest in nonmercury plasma discharges for lighting applications. In the standard low-pressure fluorescent bulb, xenon [1], or pulsed xenon-neon mixtures are under investigation as replacements for Hg [2]. Such rare gas fills require new phosphors and affect the electrode behavior [2], [3]. In high-pressure discharges, metallic zinc has been studied as a mercury replacement as it is also a group IIB element in the periodic table [4]. Very high bulb temperatures (∼1500 K) are needed to volatize the zinc. Among electrodeless systems, the sulfur lamp [5], [6] and the cluster lamp, composed of oxi-halides [7], [8], provide Hg-free visible light by microwave generation.

On board U.S. Navy vessels, Hg is treated as hazardous material. Spent fluorescent bulbs must be stored at sea which consumes precious cargo space. The Naval Research Laboratory (NRL) is presently investigating an electrodeless, Hg-free, molybdenum-oxide-argon discharge for high intensity lighting applications [9]. The concept is similar to a metal-halide lamp except that oxygen takes the place of the halide, no Hg is involved, and it is run at a low pressure. The volatile property of metal-oxides has also been employed in a high-intensity,

high-pressure NbO lamp as discussed by Lapatovich *et al.* [10], [11], but their device includes Hg.

This paper begins with a description of the Hg-free, molybdenum–oxide–argon (Mo–O–Ar) discharge operation in the next section to provide a backdrop for the modeling work. In Section III, a zero-dimensional (0-D) model for the global properties of the discharge is developed based on the electron Boltzmann equation, particle, and thermal gas balance relations. Section III also presents results from the calculations. Section IV compares the model with interferometric measurements for the electron density and spectroscopic emission line ratios for the atomic Mo density. Section V discusses the limitations of the present model and comments on the discharge as a lamp.

II. DISCHARGE SPECTRA

The Mo–O–Ar discharge is ignited within a quartz bulb of inner diameter ∼2.3 cm and length 2.5 cm. The bulb is charged with MoO_3 powder, attached to a vacuum system through a long narrow stem, and then cleaned with a weak Ar discharge and evacuated to 10^{-5} torr to remove contaminants such as water. The bulb is back filled at room temperature with Ar at 1 torr and mechanically closed with a quartz plug through a vacuum translator. While the pump system is valved off, the plug closure is not tight, so the bulb, its stem, and an antechamber in front of the valve housing an MKS Instruments baratron capacitance manometer are similarly pressurized. An inductive discharge is initiated in the Ar buffer via a spiral coil driven by a 13.56-MHz RF generator. The coil has an inductance of 2 μH and a resistance of 0.7 Ω as determined from a Boonton Radio Corporation *Q*-meter. An automatic dual capacitor network is used for proper matching. Typical electrical parameters across the coil are ∼7 A (rms) from a Pearson current monitor, ∼1.1 kV from a capacitive voltage divider, and ∼250 W from a Bird RF Power Analyzer. Of this forward power, ∼34 W is dissipated in the copper coil. Since the vapor pressure of MoO_3 is 1 torr at 1007 K and 20 torr at 1058 K, the Mo–O undergoes a sudden evaporation from the quartz walls as they heat up. Despite the temperature rise in the discharge, the bulb's total pressure remains close to ∼1 torr as the baratron indicates a slight pressure rise consistent with the volume ratio between the bulb and the antechamber. Once evaporated into the plasma, kinetic reactions dissociate the MoO_3, and the Mo atom, excited by electron collisions, radiates in the near UV and throughout the visible domain.

During operation, Mo and its ion diffuse from the excitation region in the plasma back toward the bulb wall. At high power, most of the wall remains hot, ∼1000 K, and we observe no wall
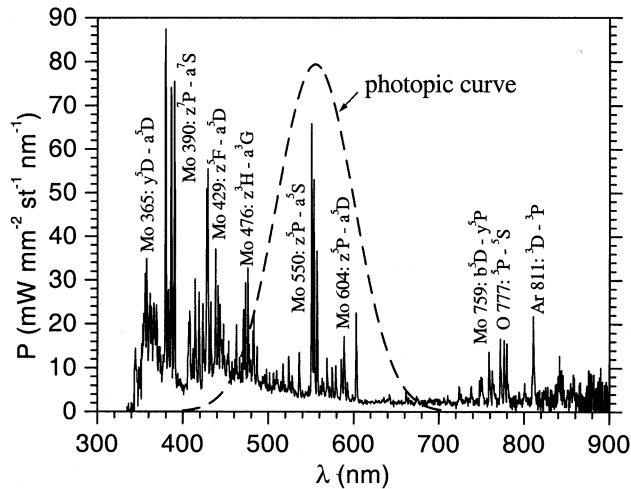
Fig. 1. Calibrated spectrum from a Mo–O electrodeless discharge with Ar as a buffer gas. Dominant emission lines are noted as well as the relative eye sensitivity.

Fig. 2. Energy level structure used for the atomic species Ar, O, and Mo in the kinetics model.

deposition of Mo over such regions. Apparently, any Mo which does condense on the hot wall is rapidly oxidized to MoO_3 and the metal-oxide reenters the gas phase to once again be dissociated and excited by electrons. This regenerative mechanism is effective except at the stem, which is the cold spot. Usually a white film (MoO_3) appears and the plug serves to keep the Mo–O from diffusing down the stem. In some cases, which conditions have not been clarified, an equilibrium is established between the cold spot and the plasma and the spectra remains fairly constant. In other experiments, the cold spot continues to accumulate material and the bulb gradually fades in visible light over tens of minutes.

A sample spectrum is shown in Fig. 1. The data were taken with an Ocean Optics Model PC2000 spectrometer. The bulb emission is focused through a 1:1 optics system with a fixed aperture onto a fiber optic and recorded on a computer. The raw data count has been absolutely calibrated for the spectral response of the optics train using the OL550 standard of spectral radiance from Optronic Laboratories. The identification of the prominent emission lines and the term designations in the spectrum of Fig. 1 are taken from the list of Whaling *et al.* [12]. The resonant transitions of MoI occur from the z^7 and y^7 septet levels near 390 nm to the ground level ($a^7 S$). Another important UV transition occurs at 320 nm, but it is beyond the sensitivity of the present spectrometer. Most of the visible emission lines are between quintet states (z^5 and y^5 to a^5). Thus, the relevant excitation path is from the ground state to the z^7 and y^7 states, followed by a collisional exchange to the z^5 or y^5 levels, and then a radiative decay leading to visible emission. The nondimensionalized photopic response function, which represents the sensitivity of the human eye, is represented in the figure as the dashed line. Note that the Mo 550 line is located very near the peak of the eye sensitivity. We can obtain an estimate of the efficacy for the Mo–O–Ar discharge by integrating the observed spectrum over wavelength weighted by the dimensional photopic response curve in lumens per watt of emitted light. Assuming that the surface emission from the bulb is the same at all points and including an angular dependency factor for the in-
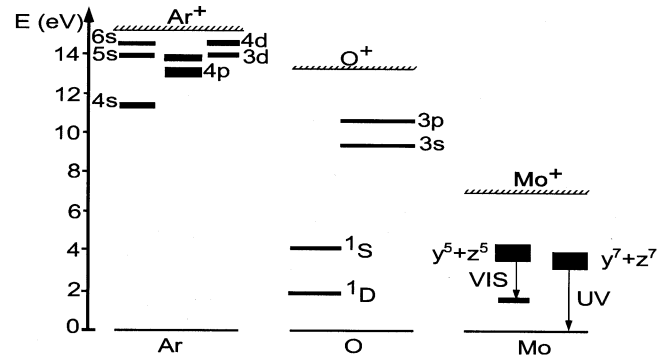
tensity, we estimate a total lumen output of $\sim 10^4$ lumens. The procedure was checked against the electrodeless Hg fluorescent Philips Q-lamp and was found to reproduce the stated output of 6000 lumens to within $\sim 10\%$. Admittedly the technique is approximate, subject to the assumption of uniform emission which may not hold for the present discharge. Adopting the previous estimate and the measured electrical input power to the inductive coil plus plasma of 250 W, gives an efficacy of ~ 40 lm/W for the Mo–O–Ar discharge.

III. GLOBAL DISCHARGE MODEL

A. Model Components

The electrodeless Mo–O–Ar discharge is a complex physical system involving electromagnetic coupling, plasma formation, wall evaporation of MoO_3, gas phase chemistry, electron dissociation, excitation and ionization, and spectral-light emission. The present model focuses on the global properties of the discharge resulting from the electron energy distribution function (EEDF) and the atomic species production within a 0-D framework. The EEDF is calculated from the time-independent homogeneous electron Boltzmann equation, using the conventional two-term expansion in Legendre polynomials. The ratio of the electric field to the neutral density (E/n) and the electron density (n_e) are starting parameters for the Boltzmann equation, and their values are calculated self-consistently. E/n is adjusted from iteration to iteration so that the electron loss through diffusion, attachment, etc., equals the electron production through ionization. Since the latter is a function of E/n, there is a unique value (eigenvalue) of E/n for which ionization balances the electron loss exactly for the chosen n_e. Based on this value for the parameter E/n the power per electron, θ_e, is obtained from the Boltzmann equation and the electron density is given by $n_e = P_w/\theta_e$, where P_w is the absorbed power density. An outer iteration continues until convergence on the electron density is achieved. Thus, at the end of the numerical approach, the power dissipated by electrons matches the power input.

A sketch of the excitable levels of the atomic species Ar, O, and Mo is shown in Fig. 2. The dominant species is argon and the lumped configurations used in the model include Ar(ns) (n = 4, 5, 6), Ar(np) (n = 4, 5) and Ar(nd) (n = 3, 4). For the oxygen atom, four excited states are considered: the two

TABLE I
REACTIONS, CROSS SECTIONS, AND TRANSITION RATES USED FOR Mo

reaction	ΔE (eV) or λ (nm)	σ (cm^{-2}) or A (1/s)	ref.
excitation			
$Mo(a^7S) + e \rightarrow Mo(y^7+z^7) + e$	3.17 (a)	$5.0 \times 10^{-15} f_1(x)$	[42] (b,c)
$Mo(a^7S) + e \rightarrow Mo(y^5+z^5) + e$	3.88	$2.9 \times 10^{-17} f_1(x)$	[42] (b,c)
$Mo(y^7+z^7) + e \rightarrow Mo(y^5+z^5) + e$	0.71	1.0×10^{-15}	(see text)
ionization			
$Mo(a^7S) + e \rightarrow Mo^+ + 2e$	7.10	$6.2 \times 10^{-16}(x-1)$	[43] (b)
$Mo(y^7+z^7) + e \rightarrow Mo^+ + 2e$	3.93	$4.2 \times 10^{-15} f_2(x)$	[44] (b,d)
$Mo(y^5+z^5) + e \rightarrow Mo^+ + 2e$	3.22	$6.3 \times 10^{-15} f_2(x)$	[44] (b,d)
radiative decay			
$Mo(y^7+z^7) \rightarrow Mo(a^7S) + h\nu$	390 (e)	6.6×10^8	[12]
$Mo(y^5+z^5) \rightarrow Mo(a^7S^*) + h\nu$	550	1.6×10^8	[12] (f)
$Mo(y^5+z^5) \rightarrow Mo(a^7S) + h\nu$	346	4.6×10^6	[12]

a) Threshold energies ΔE for excitationa and ionization from Ref.[12].
b) $x = \epsilon/\Delta E$ where ϵ is the electron kinetic energy.
c) $f_1(x) = (x-1)x^{-2}ln(1.25x)$.
d) $f_2(x) = (3.25+x)^{-1}[5/3 - 1/x - 2/(3x^2)]$.
e) Transition wavelengths for radiative decay taken for the strongest line in each of the lumped levels from Ref.[12].
f) The wavelength represents a decay to quintet metastable levels, which are not followed.

metastable states ^1S and ^1D and two groups of levels, namely 3 s and 3 p. The electronic structure of neutral Mo is extremely rich containing about 2000 energy levels. Based on the excitation and emission pathways discussed in the previous Section, a simplified atomic structure for Mo is adopted consisting of two lumped excited states, vis., the resonance levels $Mo(y^7+z^7)$ and the dominant optically emitting levels $Mo(y^5+z^5)$. Excited states of O_2 were not taken into account, however inelastic electron collisions involving the ground state of O_2 are considered, such as vibrational and electronic excitation, dissociation, and attachment, in order to account for the power losses. The ionized species Ar^+, Ar_2^+, Mo^+, O^+, O_2^+, O^-, and O_2^-, are included in their ground states.

We assume that there are no MoO_x molecules in the emitting region of the plasma, i.e., the Mo–O is readily dissociated as it evaporates from the hot-bulb wall. At a fixed Ar pressure and input power, the Mo pressure is treated as an input parameter. This pressure is defined by the total density of Mo containing species, $p_{Mo} = k_B T_g(n_{Mo(a^7S)} + n_{Mo(y^5+z^5)} + n_{Mo(y^7+z^7)} + n_{Mo^+})$, where k_B is the Boltzmann constant and T_g is the gas temperature. By nuclei conservation $n_O^{nuc} = 3n_{Mo}^{nuc}$, where n_O^{nuc} includes the density of the five states in neutral oxygen of Fig. 2, the ions O^+ and O^-, and twice the density of the molecules O_2, O_2^+, O_2^-. The division between O and O_2 is determined by balancing the electron impact dissociation with molecule formation at the bulb wall. Mo may be partially ionized or have a high degree of ionization. The division between Mo and Mo^+ depends on the ionization rate of Mo and the ambipolar diffusion of Mo^+. The electrons and positive ions are lost by dissociative recombination and at the tube wall through ambipolar diffusion. The positive ions are also lost in ion–ion recombination. The negative ions are assumed to be lost in volume recombinations only. The populations of the excited states of Ar, O, and Mo are determined with a collisional-radiative model involving numerous gas-phase reactions.

The cross sections for elastic and inelastic collision processes of electrons with Ar [13]–[16], O [17]–[19], and O_2 [20] are specified elsewhere. This data is used in the collision term of the Boltzmann equation. The chemical and wall reactions between neutral and charged oxygen species can also be found in the literature [21]–[29]. Recent kinetic models and experiments in Ar–O_2 plasmas indicate the relevant kinetic processes in this mixture [30]–[33], the most important being the Penning ionization and charge transfer [34]–[39]. To our knowledge, the only kinetics model for Mo in the literature is that of Guimaraes *et al.* [40], [41]. The authors used Drawin's formula to estimate the electron impact excitation cross sections from the ground state of Mo. We followed the same procedure to estimate one lumped cross section to the septet state and one to the quintet states. In addition, we included transitions between the septet and quintet states of Mo due to electron collisions, assuming a rate coefficient 10^{-7} cm^3/s. Table I presents a list of the reactions, cross sections, and radiative transitions used for the Mo kinetics. The reaction constants are derived from formulas provided by the the the listed references. The radiation has been treated using the probability-of-escape formalism in the on-the-spot approximation. The escape factors provide effective lifetimes for the radiative transitions and depend on the lower state density, the gas temperature, and the bulb dimensions. The general formulas for the escape factors are taken from [45].

In addition to the species balance and electron Boltzmann equations, the gas thermal balance equation is solved in the model. The analytic solution is a Bessel profile for $T_g(r)$. The source terms, which are taken as spatially uniform, include elastic heating by electrons as well as the energy lost by electrons through vibrational excitation and dissociation of O_2. The boundary condition at the axis is a zero temperature gradient while at the bulb wall, $T_g = T_{wall}$. The wall temperature T_{wall} is estimated from the power flux to the wall, P_{wall}, comprising gas thermal conduction and species diffusion: $P_{wall} = \sigma_{SB}(T_{wall}^4 - T_o^4)$. Here, T_o is room temperature and σ_{SB} is the Stefan–Boltzmann constant. The gas temperature reported for the model is the radially averaged value. The wall temperature is typically computed to be 800 K–900 K.
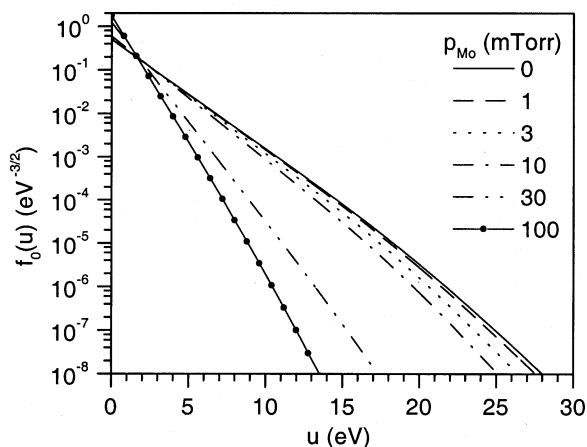
Fig. 3. Normalized electron energy distribution function at various partial pressures of Mo. The plasma conditions are an Ar pressure of 1 torr and a coupled power density of 24 W/cm^3.
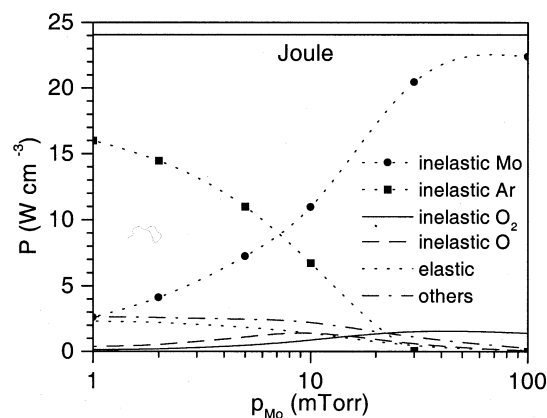
Fig. 4. Power density transfer from electrons into various channels and species. Total power density and Ar pressure are the same as in Fig. 3.
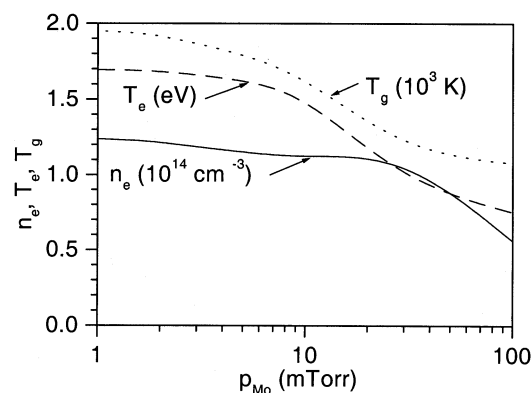
Fig. 5. Electron temperature, gas temperature, and electron density as a function of the Mo partial pressure. Total power density and Ar pressure are the same as in Fig. 3.

B. Model Results

The calculations presented in the following pertain to a bulb with an Ar pressure of 1 torr and a total power coupled to the plasma of 250 W. Given a cylindrical bulb of radius 1.15 cm and length 2.5 cm, this translates to a power density of $P_w = 24$ W/cm^3. Properties of the discharge are investigated as a function of the partial pressure of atomic molybdenum, p_{Mo}, as defined previously. This approach is similar to that used in modeling the standard fluorescent bulb wherein the partial pressure of mercury is varied.

Fig. 3 displays the EEDF which is normalized over the electron energy u such that $\int f_o(u)\sqrt{u}\,du = 1$. A Maxwellian distribution would be a straight line in this plot. At low values of p_{Mo}, the EEDF departs from a Maxwellian above the ionization potential of Ar (15.8 eV), but as p_{Mo} increases the EEDF becomes completely Maxwellian and the mean electron energy decreases. This results from two effects. First, the energy threshold for inelastic losses due to collisions with Mo is significantly smaller than with Ar (see Fig. 2). As p_{Mo} increases, these collisions extract energy from the electron distribution and lower the mean electron energy. Second, the relaxation time toward a Maxwellian distribution is shorter for a lower mean energy. The importance of the Mo abundance on the EEDF can also be ascertained by examining the channels through which the electrons transfer their energy to the gas. The transfer rate can be computed from the solution to the Boltzmann equation. In Fig. 4, the inelastic channels are summed according to the recipient species and compared with the elastic transfer to the gas. At $p_{Mo} = 1$ mtorr, the power is predominantly lost from the electrons through inelastic collisions with Ar. Excitations of Mo and O as well as elastic processes, though comparable to each other, are smaller than the Ar losses by a factor of $\sim$6. As the partial pressure of Mo increases, there is a rapid transition away from inelastic losses with Ar to those with Mo. Simultaneously, inelastic losses to O$_2$ increase while all others, including elastic losses, decrease at high Mo abundance. Losses to O and O$_2$ are always less than losses to Mo. As before, this shift in the energy transfer is due to the large collisional excitation rate of Mo. Hence, at some abundance the power transfer must predomi-

nantly go into Mo and the calculations indicate that this occurs at $p_{Mo} \sim 7$ mtorr. Between 10 and 30 mtorr of Mo, collisional losses to Ar becomes negligible and this effect is associated with the cooling of the EEDF seen in Fig. 3.

The electron temperature T_e, which is 2/3 the mean energy, is presented in Fig. 5 as a function of p_{Mo} along with the electron density n_e and the gas temperature T_g. Since the electron temperature noticeably decreases above $p_{Mo} \sim 10$ mtorr, there is a decrease of T_g as the energy exchange rate from the electrons to the gas due to elastic collisions is proportional to $T_e - T_g$. The electron density is also seen to decrease as p_{Mo} increases. At first, this seems surprising as the ionization potential of Mo is only 7.1 eV and an increase in the Mo abundance should lead to a higher ionization fraction. While it is true that the dominant ion becomes Mo$^+$ at large p_{Mo} (see the following), the power cost per ion–electron pair, $\theta_e = P_w/n_e$, is not constant but rather increases with the Mo fraction due to inelastic collisions involving low energy electrons. In particular, θ_e changes from 2×10^{-13} to 4×10^{-13} W/e$^-$ as p_{Mo} increases by two orders of magnitude. The excessive power loss in inelastic collisions with Mo overcompensates the lower ionization potential of Mo and the electron density decreases. Using the momentum transfer rate constant of 2×10^{-8} cm^3/s at $T_e = 1$ eV, the collision frequency at 1 torr of Ar is seven times larger than the angular RF frequency at 13.56 MHz. In this regime, the classical
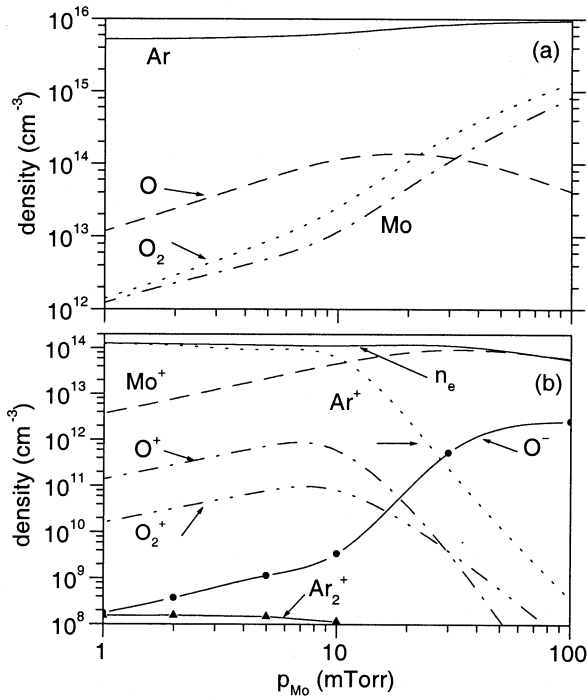
Fig. 6. Calculated number densities of (a) neutral and (b) ionized species as a function of the Mo partial pressure. Total power density and Ar pressure are the same as in Fig. 3.

Fig. 7. Measured electron density as a function of coupled power for pure Ar (circles) and for MoO_3–Ar (squares) discharges. The power per electron is denoted for the latter set.

skin depth δ describes the inductive coupling. Over the range of p_{Mo} in Fig. 5, δ increases from ~ 0.2 to ~ 0.3 cm. This is four to six times smaller than the bulb radius and suggests that the deposition is restricted to an outer plasma envelope.

The neutral and ionized species densities n_X are presented in Fig. 6. Note that the Ar density changes inversely with T_g since its pressure is maintained at 1 torr in the model. Also, the neutral Mo density is not linear with p_{Mo} as the latter includes ions as well as changes in the gas temperature from Fig. 5. At low Mo pressure nearly all of the molybdenum is in the ionized state. However, since the Mo density is less than that of the electrons, Ar^+ is the dominant ion. As p_{Mo} increases the dominant ion transitions from Ar^+ to Mo^+ at $p_{Mo} \sim 10$ mtorr. This transition stems from the cooling of the EEDF at high p_{Mo} in conjunction with the lower ionization potential of Mo compared to Ar or O. At high p_{Mo} all of the electropositive ions are Mo^+ and there is a few percent of O^-. In this regime, the Mo density is greater than that of the electrons, and most of the Mo is in the neutral state. For oxygen an analogous effect to the ionization degree of Mo is observed only for dissociation. At low p_{Mo}, oxygen is a negligible fraction of the neutral species and, as $n_e > n_O^{nuc}$, nearly all of the oxygen is dissociated. At high Mo pressure the oxygen is more abundant than the electrons and only a fraction is dissociated. A similar effect is observed for nitrogen in a He–N_2 discharge [46].

IV. COMPARISON WITH DATA

According to Figs. 4–6, one of the key parameters controlling the Mo–O–Ar discharge is the abundance of Mo. The model indicates that between 10 and 30 mtorr of Mo, the electron
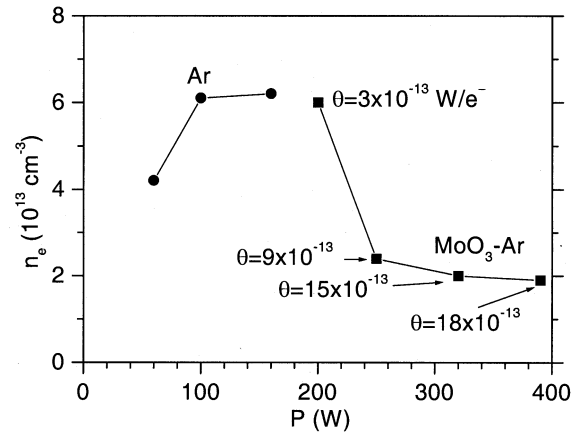
temperature decreases, the dominant channel for power deposition switches from Ar to Mo, Mo^+ becomes the dominant ion, and the electron density begins to decrease. While p_{Mo} cannot be independently adjusted in the experiment, the Clausius–Clapeyron equation [47] states that the vapor pressure of MoO_3 is exponentially dependent on the wall temperature T_{wall}. Presumably, in the experiment, a higher coupled power to the plasma raises T_{wall} and releases more oxide into the plasma for dissociation. Thus, one can measure the variation of the electron density as a function of power and relate the data to the above modeling.

The electron density was measured using a microwave interferometer at 140 GHz. The transmitting leg of the interferometer circuit included focusing horns and a variable attenuator. The reference leg had a variable phase shifter as well as an attenuator. The two signals were combined in a short slot hybrid coupler and two crystal detectors from Millitech (DXP-08) were used to monitor the signals. The nonlinear response of each detector was calibrated with a power meter following the procedure of Hotston and Seidl [48]. The measurements were made by interrupting the RF while triggering the oscilloscope to record the detector signals as the plasma decayed. The approach of Lindberg and Eriksson [49] was adopted to treat phase changes greater than π.

Results for n_e as a function of power at an Ar pressure of 1 torr are presented in Fig. 7. In the pure Ar discharge, n_e saturates at $\sim 6 \times 10^{13}$ cm^{-3} as the power increases. This value is about a factor of two less than the calculated electron density in Fig. 5. The model is apparently not accounting for all of the power losses from the electrons and θ_e should be larger than 2×10^{-13} W/e$^-$. In the Mo–O–Ar discharge of Fig. 7, one sees that n_e decreases with power. This is similar to the decrease in n_e with p_{Mo} calculated for Fig. 5, if one makes the correspondence between power and Mo partial pressure. Furthermore, the visible light emission in the experiment dramatically increased by nearly an order of magnitude between 200 and 250 W. The spectrum for the latter power is shown in Fig. 1. This increase in Mo emission is likewise consistent with the transition in Fig. 4 from an Ar dominated discharge at low p_{Mo} to a Mo dominated one at high values of p_{Mo}. Based on the trends of the model in
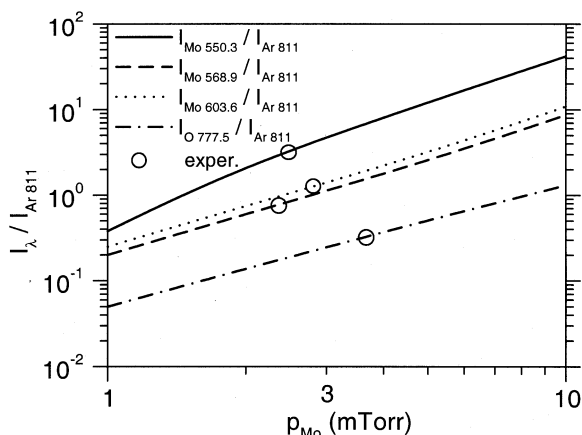
Fig. 8. Comparison of several line intensity ratios, calculated from the model as a function of Mo partial pressure, with those from spectral measurements. The latter ratios are denoted by circles. Total power density and Ar pressure for both the model and the experiment are 250 W and an Ar pressure of 1 torr.

Figs. 4 and 5, a rough estimate for the Mo partial pressure at the 250 W experimental point is between 10 and 100 mtorr.

The model can also be employed in conjunction with spectral line measurements to obtain a more direct estimate of the Mo density. The approach is a variation of the standard actinometry method for abundances [50] except that the assumption limiting excitation of the emitting level from only the ground state is not necessary. The populations of the atomic levels displayed in Fig. 2 were combined with transition probabilities to calculate synthetic intensity ratios. For the measurements, the optical configuration used to obtain the broadband spectrum of Fig. 1 was employed with separate gratings and fibers for the visible and near infrared regimes. Correction for the spectral response function across the regimes was accounted for. The emission intensity of three Mo lines under the photopic curve along with one O line in the infrared were compared against the strong 811.75-nm Ar emission lines from the $2p_9$ to the $1s_5$ Paschen levels.

Fig. 8 displays the calculated ratios of O 777 nm and several Mo lines to the Ar 811-nm line at different Mo pressures. The discharge parameters are 250-W total coupled power and 1-torr Ar pressure. The measured ratios of the same line intensities are taken with the same experimental conditions and denoted in the figure. The comparison indicates that the partial pressure of Mo is between 2 and 4 mtorr, significantly smaller than the previous estimate based on the transition from an Ar to a Mo dominant discharge. In this low-Mo pressure domain, the model results indicate that most of the molybdenum is ionized and much of the power would be dissipated in excitations of Ar.

V. DISCUSSION AND CONCLUSION

We have presented a first-order global model of a Mo–O–Ar discharge using the Boltzmann equation and compared the results with some observations. The primary conclusion from the model calculations is a transition in the nature of the discharge as the partial pressure of moly is increased. This transition is characterized by a decrease in the electron temperature (Fig. 3), a power transfer from Ar excitation to Mo excitation (Fig. 4), a decrease in the electron density (Fig. 5), and a replacement of Ar^+ as the dominant ion to Mo^+ simultaneous with a reduc-

tion in the degree of ionization of molybdenum (Fig. 6). Such a transition is observed in the experimental discharge bulb as the coupled power is increased. At 200 W, the bulb displays weak emission dominated by Ar lines, but at 250 W, the visible output increases by an order of magnitude and the spectrum shows strong emission lines from Mo (Fig. 1). The power deposition is related to evaporation of MoO_3 from the bulb's inner surface through a corresponding increase in the wall temperature. At a particular Mo fraction, the power transfer from the electrons is switched from excitation of the Ar resonance lines in the deep UV to excitation of the Mo resonant septet levels in the near UV and the associated pumping of the quintet levels leading to visible emission. The Mo excitation rate is larger than for Ar and the power per ion–electron pair decreases as observed in Fig. 7. We also note that the global discharge parameters from Fig. 5 indicate a nonequilibrium plasma with $T_e \gg T_g$. This is to be expected due to the low pressure ($\sim$1 torr) of the discharge, but is also qualitatively supported by the observed spectrum which shows Ar emission lines simultaneously with those from Mo (Fig. 1). Emission lines from Ar arise from levels $\sim$13 eV above the ground state which require electrons energies of $\sim$1 eV or more. On the other hand, the quartz bulb cannot be this hot but must be above 800 K in order for MoO_3 to have a vapor pressure of at least 1 mtorr.

While there is qualitative agreement between the model and the data, the quantitative comparison shows significant differences. The calculated electron density of Fig. 5 is a factor of two larger than the measured value from the microwave interferometry in Fig. 7. Furthermore, the value for the Mo partial pressure at the transition is between 10 and 30 mtorr based on Fig. 4, but a comparison of line ratios between the model and data in Fig. 8 indicate a lower range, between 2 and 4 mtorr. The nature of these differences suggest particular areas where the model needs to be improved. First, nonequilibrium discharges containing metals with open nd- and $(n + 1)$ s-shells, such as Mo, are a challenge for kinetic calculations due to the large number of energy levels (about 2000 in neutral Mo). The approach taken here was limited to the Mo excitation path leading to emission near 550 nm. An improved atomic level structure would include more electron configurations, lumped in an appropriate manner, with exchange collisions and excitations to the individual quintet states. Cross sections for these electron collisions would need to be calculated rather than estimated as done in Section III-A. The additional channels would raise the power per ion–electron pair, θ_e, to be more consistent with the experimental values denoted in Fig. 7 which are greater than the model predicts. At a fixed power deposition, the electron density would then be lower. Second, the evaporation of MoO_3 from the bulb walls and the subsequent dissociation by gas phase reactions or electron impact need to be treated in some detail. The rate constants for MoO_X $(X = 1, 2, 3)$ dissociation are not well known but might be approximated from reactions involving other similar molecules. This treatment would establish a self-consistent coupling between the power deposition, the wall temperature, and the partial pressure of molybdenum. Proper implementation of the heat-flux calculation leads to the third improvement, a 1-D model. This would also allow one to account for the electromagnetic skin depth and multispecies diffusion near the bulb wall.

In terms of the Mo–O–Ar discharge as a potential compact electrodeless light source, Fig. 1 indicates that metallic emission is the dominant contributor to the visible light. The same property is true for high-pressure metal-halide arc lamps, but the plasma properties are quite different. Halide lamps operate in a Hg vapor pressure of several atmospheres under thermodynamic equilibrium conditions. The present low-pressure, Hg-free, nonequilibrium discharge has attained an efficacy of ∼40 lm/W, similar to the high pressure Hg–NbO of [11]. For use in general lighting, the efficacy could be increased by converting the near UV emission seen in Fig. 1 to visible light through a phosphor. From [12], the strongest UV transitions are near 320 and 390 nm. The standard phosphor used in fluorescent lamps are not effective at converting such radiation into visible light, so alternative phosphors would be required. Based on the present Mo kinetics model of Table I, we find that the emission in the near UV can be up to 1.6 times larger than the visible emission, or about 60 W. An alternative approach would be to increase the Mo density or the addition of other absorbing metals into the discharge such that the UV resonance lines become optically thick. This could enhance the transitions in the visible region of the spectrum relative to the UV component.

REFERENCES

[1] D. A. Doughty, "Discharge paths to mercury-free lighting," in *Proc. 50th Annu. Gaseous Electronics Conf., Bull. Amer. Phys. Soc.*, vol. 42, 1997, p. 1702.

[2] M. Jinno, H. Kurokawa, and M. Aono, "Fundamental research on mercuryless fluorescent lamps. I—Inner electrode operation with pulsed discharge," *Jpn. J. Appl. Phys.*, vol. 38, pp. 4608–4612, 1998.

[3] J. M. Depond, "High voltage, mercury-free fluorescent lamps with cold cathodes: State of art and future developments," in *Proc. IEEE Ind. Applicat. Conf.*, vol. 5, 2000, pp. 3322–3325.

[4] M. Born, "Investigations on the replacement of mercury in high-pressure discharge lamps by metallic zinc," *J. Phys. D, Appl. Phys.*, vol. 34, pp. 909–924, 2001.

[5] M. G. Ury, B. P. Turner, and J. T. Dolan, "Sulfur discharges as high efficacy light sources," in *Proc. IEEE Conf. Plasma Science*, 1993, p. 219.

[6] B. Cook, "New developments and future trends in high-efficiency lighting," *Eng. Sci. Educ. J.*, vol. 9, pp. 207–217, 2000.

[7] R. Weber and R. Scholl, "A new kind of light-generation mechanism: Incadescent radiation from clusters," *J. Appl. Phys.*, vol. 74, pp. 607–613, 1993.

[8] M. Heintel, M. Neiger, and R. Scholl, "Investigation of the radiation mechanism of microwave excited cluster lamps," *Contrib. Plasma Phys.*, vol. 38, pp. 419–433, 1998.

[9] V. A. Shamamian, D. J. Vestyck Jr., J. L. Giuliani, and J. E. Butler, "Metal oxide discharge lamp," U.S. Patent 6 157 133, Dec. 5, 2000.

[10] W. P. Lapatovich, W. M. Keeffe, N. Brates, R. W. Liebermann, and J. Maya, "Metal oxide containing high intensity discharge lamps," in *Proc. 4th Int. Symp. Science and Technology of Light Sources*, 1986, p. 277.

[11] ——, "High intensity discharge device containing oxytrihalides," U.S. Patent 4 672 267, June 9, 1987.

[12] W. Whaling, P. Hannaford, R. M. Lowe, E. Biemont, and N. Grevesse, "Lifetimes, branching ratios, and transition probabilities in MoI," *J. Quantum Spectrosc. Radiat. Transf.*, vol. 32, pp. 69–80, 1984.

[13] C. M. Ferreira and J. Loureiro, "Electron transport parameters and excitation rates in Ar," *J. Phys. D, Appl. Phys.*, vol. 16, pp. 1611–1621, 1983.

[14] A. Bogaerts, R. Gijbels, and J. Vlcek, "Collisional-radiative model for an argon glow disvharge," *J. Appl. Phys.*, vol. 84, pp. 121–136, 1998.

[15] G. M. Petrov and C. M. Ferreira, "A Collisional-radiative model for argon discharges at intermediate and high pressures," Instituto Superior Técnico, Lisbon Tech. Univ., Lisbon, Portugal, Internal Rep. CFP 10/97, 1997.

[16] M. Petrov, J. L. Giuliani, and A. Dasgupta. (2002) Electron energy deposition in an electron-beam pumped KrF amplifier: Impact of beam power and energy. *J. Appl. Phys*, pp. 2662–2677.

[17] Y. Itikawa and A. Ichimura, "Cross sections for collisions of electrons and photons with atomic oxygen," *J. Phys. Chem. Ref. Data*, vol. 19, pp. 637–651, 1990.

[18] S. S. Tayal and R. J. W. Henry, "Electron-impact excitation of atomic oxygen," *Phys. Rev. A, Gen. Phys.*, vol. 38, pp. 5945–5948, 1988.

[19] S. P. Slinker, R. D. Taylor, and A. W. Ali, "Electron energy deposition in atomic oxygen," *J. Appl. Phys.*, vol. 63, pp. 1–10, 1988.

[20] S. Kajita, S. Ushiroda, and Y. Kondo, "Influence of the dissociation process of oxygen on the electron swarm parmeters in oxygen," *J. Appl. Phys.*, vol. 67, pp. 4015–4023, 1990.

[21] Y. Ichikawa and R. L. C. Wu, "Theoretical and experimental characterization of positive column plasmas in oxygen glow discharge," *J. Appl. Phys.*, vol. 67, pp. 108–114, 1990.

[22] M. A. Lieberman and A. J. Lichtenberg, *Principles of Plasma Discharges and Materials Processing*. New York: Wiley, 1994, p. 398.

[23] V. A. Feoktistov, A. V. Mukhovatova, A. M. Popov, and V. T. Rakhimova, "Self-consistent modeling of low-pressure rf discharges in oxygen plasma," *J. Phys. D, Appl. Phys.*, vol. 28, pp. 1346–1353, 1995.

[24] B. F. Gordiets, C. M. Ferreira, V. L. Guerra, J. M. A. H. Loureiro, J. Nahorny, D. Pagnon, M. Touzeau, and M. Vialle, "Kinetic model of a low-pressure N_2-O_2 flowing glow discharge," *IEEE Trans. Plasma Sci.*, vol. 23, pp. 750–768, Aug. 1995.

[25] V. Guerra and J. Loureiro, "Self-consistent electron and heavy-particle kinetics in a low-pressure N_2-O_2 glow discharge," *Plasma Sources Sci. Technol.*, vol. 6, pp. 373–385, 1997.

[26] M. J. Pineiro, G. Gousset, A. Granier, and C. M. Ferreira, "Modeling of low pressure surface wave discharge in flowing oxygen: I. Electrical properties and species concentration," *Plasma Sources Sci. Technol.*, vol. 7, pp. 524–536, 1998.

[27] M. Capitelli, C. M. Ferreira, B. F. Gordiets, and A. I. Osipov, *Plasma Kinetics in Atmospheric Gases*. Berlin, Germany: Springer-Verlag, 2000, pp. 180–182 and 185.

[28] S. Panda and D. J. Economou, "Effect of metastable oxygen molecules in high density power-modulated oxygen discharges," *J. Appl. Phys.*, vol. 87, pp. 8323–8333, 2000.

[29] J. T. Gudmundsson, I. G. Kouznetsov, K. K. Patel, and M. A. Lieberman, "Electronegativity of low-pressure high-density oxygen discharges," *J. Phys. D, Appl. Phys.*, vol. 34, pp. 1100–1109, 2001.

[30] W. Trennepohl Jr., J. Bretagne, G. Gousset, D. Pagnon, and M. Touzeau, "Modeling of an Ar-O_2 reactive magnetron discharge used for deposition of chromium oxide," *Plasma Sources Sci. Technol.*, vol. 5, pp. 607–621, 1996.

[31] S. Rauf and M. J. Kushner, "Argon metastable densities in radio frequency Ar, Ar/O_2, and Ar/CF_4 electrical discharges," *J. Appl. Phys.*, vol. 82, pp. 2805–2813, 1997.

[32] K. Nanbu, K. Mitsui, and S. Kondo, "Self-consistent particle modeling of dc magnetron discharge in O_2/Ar mixture," *J. Phys. D, Appl. Phys.*, vol. 33, pp. 2274–2283, 2000.

[33] J. T. Gudmundsson, T. Kimura, and M. A. Lieberman, "Experimental studies of O_2/Ar plasma in a planar inductive discharge," *Plasma Sources Sci. Tech.*, vol. 8, pp. 22–30, 1999.

[34] L. G. Piper, J. E. Velazco, and D. W. Setser, "Quenching cross sections for energy transfer reactions between metastable argon atoms and noble gases and small molecules," *J. Chem. Phys.*, vol. 59, pp. 3323–3340, 1973.

[35] D. Smith, C. V. Goodall, N. G. Adams, and A. G. Dean, "Ion- and electron-density decay rates in afterglow plasmas of argon and argon-oxygen mixtures," *J. Phys. B, At. Mol. Opt. Phys.*, vol. 3, pp. 34–44, 1970.

[36] G. D. Flesch, S. Nourbakhsh, and C. Y. Ng, "Absolute state-selected and state-to-state total cross sections for the reaction $Ar^+(^2P_{3/2,1/2})+O_2$," *J. Chem. Phys.*, vol. 92, pp. 3590–3604, 1990.

[37] C. Rebrion, B. R. Rowe, and J. B. Marquette, "Reactions of Ar^+ with H_2, N_2, O_2, and CO at 20, 30, and 70 K," *J. Chem. Phys.*, vol. 91, pp. 6142–6147, 1989.

[38] A. J. Midey and A. A. Viggiano, "Rate constants for the reaction of Ar^+ with O_2 and CO as a function of temperature from 300 to 1400 K: Derivation of rotational and vibrational energy effects," *J. Chem. Phys.*, vol. 109, pp. 5257–5263, 1998.

[39] J. W. Keto, C. F. Hart, and C.-Y. Kuo, "Electron beam excited mixtures of O_2 in argon. III. Energy transfer to O_2 and O_3," *J. Chem. Phys.*, vol. 74, pp. 4450–4454, 1981.

[40] F. Giumaraes and J. Bretagne, "Study of an argon magnetron discharge used for molybdenum sputtering. I collisional radiative model," *Plasma Sources Sci. Technol.*, vol. 2, pp. 127–137, 1993.

[41] F. Giumaraes, J. B. Almeida, and J. Bretagne, "Study of an argon magnetron discharge used for molybdenum sputtering. II spectroscopic analysis and comparison with the model," *Plasma Sources Sci. Technol.*, vol. 2, pp. 138–144, 1993.

[42] H. W. Drawin, "Influence of atom-atom collisions on the collisional-radiative ionization and recombination coefficients in hydrogen plasmas," *Z. Physik*, vol. 225, pp. 483–493, 1969.

[43] E. J. McGuire, "Electron ionization cross sections in Born approximation," *Phys. Rev. A, Gen. Phys.*, vol. 16, pp. 62–72, 1977.

[44] L. Vriens and A. H. M. Smeets, "Cross-sections and rate formulas for electron-impact ionization, excitation, deexcitation, and total depopulation of excited atoms," *Phys. Rev. A, Gen. Phys.*, vol. 22, pp. 940–951, 1980.

[45] K. Igarashi, S. Mikoshiba, Y. Watanabe, M. Suzuki, and S. Murayama, "Characterization of imprisoned Xe resonant photons in He-Xe and Ne-Xe mixtures," *J. Phys. D, Appl. Phys.*, vol. 28, pp. 1377–1383, 1995.

[46] G. M. Petrov, J. P. Matte, I. Peres, J. Margot, T. Sadi, J. Hubert, K. C. Tran, L. L. Alves, J. Loureiro, C. M. Ferreira, V. Guerra, and G. Gousset, "Numerical modeling of a He-N_2 capillary glow discharge at atmospheric pressures," *Plasma Chem. Plasma Process.*, vol. 20, pp. 183–207, 2000.

[47] P. Atkins, *Physical Chemistry*. New York: Freeman, 1998, p. 152.

[48] E. Hotston and M. Seidl, "A microwave interferometer for the measurement of small phase angles," *J. Sci. Instrum.*, vol. 42, pp. 225–230, 1965.

[49] L. Lindberg and A. Eriksson, "Optimum design of a microwave interferometer for plasma density measurments," *J. Phys. E: Sci. Instrum.*, vol. 15, pp. 548–554, 1982.

[50] S. E. Savas, "Observations of argon emission lines used for fluorine actinometry in low power rf discharges," *Appl. Phys. Lett.*, vol. 48, pp. 1042–1044, 1986.

George M. Petrov was born in Lovetch, Bulgaria, in 1965. He received the M.Sc. diploma in physics from Sofia University, Sofia, Bulgaria, in 1990 and the Ph.D. degree from the Bulgarian Academy of Science, Sofia, in 1997.

From 1994 to 1996, he was with the Institut für Niedertemperatur-Plasmaphysik, Greifswald, Germany. In 1997, he joined the Instituto Superior Técnico, Lisbon, Portugal, and in 1998, he joined the University of Montreal, Montreal, QC, Canada. Since May 1999, he has been with Berkeley Research Scholars. Inc, Springfield, VA. His current research interests include modeling of glow discharges, e-beam deposition and gas laser kinetics, and lighting.
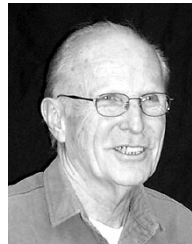
Robert E. Pechacek received the B.Sc. degree in engineering from the California Institute of Technology, Pasadena, in 1954 and the Ph.D. degree in electrical engineering from the University of California, Berkeley, in 1966.

He joined the Naval Research Laboratory (NRL), Washington, DC, in 1970 where he has conducted Z-pinch and magnetic cusp plasma confinement experiments and experiments on laser guided discharges and laser produced low density channels in air. He retired from the NRL in 1992 and returned as a Consultant with Sachs Freeman Associates, Inc., Largo, MD.

John L. Giuliani (M'91) received the B.S. degree in physics from Georgetown University, Washington, DC, in 1972 and the Ph.D. degree in theoretical astrophysics from Yale University, New Haven, CT, in 1980.

For several years, he continued research on the interstellar medium at the Institute for Advanced Study and Princeton University, Princeton, NJ. In 1983, he joined the Naval Research Laboratory (NRL), Washington, DC, where he is currently the Head of the Dense Plasma Dynamics Section. At NRL, he has worked on high-altitude nuclear effects, laser target interactions, z-pinch implosions, and strongly coupled plasmas. His current research interests include plasma materials processing, gas laser kinetics, and lighting.

Robert A. Meger (M'97–A'01) received the Ph.D. degree in applied physics from Cornell University, Ithaca, NY, in 1977.

After being a Postdoctoral Researcher at the University of Maryland, College Park for two years, he joined the Plasma Physics Division, Naval Research Laboratory, Washington, DC, where he is currently the Head of the Charged Particle Physics Branch. His research interests include applications of pulsed power, plasma opening switches, relativistic electron beam propagation, hypervelocity mass launchers, advanced radars, and plasma processing.

Dr. Meger is a Fellow of the American Physical Society.